Novelty without nobility: Outstanding Ni/Ti-SiO_2 catalysts for propylene epoxidation

J. García-Aguilar, J. Fernández-Catalá, J. Juan-Juan, I. Such-Basá ñez, L.E. Chinchilla, J.J. Calvino-Gámez, D. Cazorla-Amorós, Á. Berenguer-Murcia

PII: S0021-9517(20)30127-5
DOI: https://doi.org/10.1016/j.jcat.2020.04.006
Reference: YJCAT 13708

To appear in: *Journal of Catalysis*

Received Date: 10 March 2020
Revised Date: 3 April 2020
Accepted Date: 4 April 2020

Please cite this article as: J. García-Aguilar, J. Fernández-Catalá, J. Juan-Juan, I. Such-Basáñez, L.E. Chinchilla, J.J. Calvino-Gámez, D. Cazorla-Amorós, Aacute. Berenguer-Murcia, Novelty without nobility: Outstanding Ni/Ti-SiO_2 catalysts for propylene epoxidation, *Journal of Catalysis* (2020), doi: https://doi.org/10.1016/j.jcat.2020.04.006

Novelty without nobility: Outstanding Ni/Ti-SiO_2 catalysts for propylene epoxidation

J. García-Aguilar[1], J. Fernández-Catalá[1], J. Juan-Juan[2], I. Such-Basáñez[2], L.E. Chinchilla[3], J.J. Calvino-Gámez[3], D. Cazorla-Amorós[1], Á. Berenguer-Murcia[1].*

[1]Materials Science Institute and Inorganic Chemistry Department, University of Alicante, Ap. 99, E-03080 Alicante, Spain.

[2]Research Technical Services, University of Alicante, Ap. 99, E-03080 Alicante, Spain

[3]Department of Materials Science and Metallurgical Engineering and Inorganic Chemistry, University of Cadiz, Cadiz, Spain

ABSTRACT. An efficient gas-phase production of propylene oxide (PO) with noble metal-free catalysts could modify the industrial output of this valuable compound. We present a novel catalyst based on well-dispersed Ni nanoparticles loaded on a Ti-SiO_2 support for the propylene epoxidation reaction using H_2/O_2 mixtures. XPS, High Resolution Transmission Electron Microscopy (HRTEM), and UV-Vis corroborate both the small size of Ni particles and the

* Corresponding author: Dr. Ángel Berenguer Murcia (a.berenguer@ua.es) Tel.: +34 965 909350; Fax: +34 965 903454

excellent dispersion and incorporation of Ti as tetrahedral single site species into the silica framework. The catalytic results under steady-state conditions at low temperature (200ºC) show high PO selectivity (around 85%) with a substantial propylene conversion (over 6%) and excellent H_2 efficiency (~37%) using only 0.5 wt. % of Ni on Ti-SiO_2 (Ti/Si=0.01 molar ratio). In this work, we have also carried out a preliminary DFT study to gain understanding of the characteristics that make this nickel catalyst active and selective for the propene epoxidation reaction.

KEYWORDS. Nickel, Titanium, Silica, Single-site, Propylene, Epoxidation.

1.- INTRODUCTION

The worldwide production of propylene oxide (PO) is increasing each year due to its use as a pre-polymer for polyurethanes or polyether polyols synthesis.[1] At present, PO is mainly produced in liquid phase by the chlorohydrin process (40% of PO production) or by the organic hydroperoxide processes. However, some problems are associated to these commercial processes: for example the use of dangerous and highly oxidizing reagents, such as Cl_2 or organic peroxides (R-OOH) and the generation of by-products which are difficult of separate.[2,3] One alternative to overcome these shortcomings is to produce PO by the oxidation of propylene via heterogeneous catalysis, since this methodology can avoid the use of Cl_2 or organic peroxides enabling the use of other more sustainable and environmentally friendly reagents like H_2/O_2 or O_2.

In the last decades, the scientific community has strongly focused on gold supported on titanosilicates catalysts for PO production in gas phase ever since Haruta et al. showed that their Au/TiO_2 catalysts (gold particles dispersed in TiO_2) could perform the propylene epoxidation reaction using H_2/O_2 mixtures with very high PO selectivity (>95%) at low propylene conversions

(1%).[4] Nevertheless this Au-based catalyst suffered from a fast deactivation over time. Stangland et al. found an active and stable catalyst based on Au supported on a microporous titanium silicalite-1 (TS-1).[5] This catalyst presented a propylene conversion of 8.8% and a PO selectivity of 81% at 473 K. This type of catalyst has been studied by the scientific community until reaching a PO selectivity about 90 % with a propene conversion around 10 % at mild temperatures using H_2/O_2 mixtures. These results show that Au-based titanosilicate (Ti-SiO_2) catalysts are very interesting for propylene epoxidation. It must be noted, however, that under these conditions a PO selectivity around 90 % is mandatory both to reach and maintain since this type of catalysts present a relatively low conversion (10%).[6-9]

In this sense, in the literature there are some theoretical and experimental studies where the authors try to clarify the reaction mechanism using Au-based catalyst. The reaction mechanism of the propylene epoxidation reaction over Au-based Ti-SiO_2 is still hitherto unclear.[10] Most of the authors propose the formation of H_2O_2 or –OOH species on the Au nanoparticles surface which migrate or spill-over towards the tetrahedral Ti incorporated in the silica framework, where propylene can be adsorbed.[11,12] Then the catalytic reaction takes place between the peroxide-like species and the adjacent Ti site.[8]

With this in mind, even though Au-based Ti-SiO_2 catalyst is a good candidate for its use in the propylene epoxidation, the use of a noble metal, in this case Au, presents some drawbacks, such as high catalyst price (due largely to the use of gold), low H_2 efficiency and also relatively low propylene conversion. For this reason, it is crucial to develop a new catalyst that uses a non-noble (i.e. transition) metal as an active phase, such as Ni, Cu, or Fe among others, due to the low price of these metals with respect to noble metals. In this aspect, one alternative can be the use of Ag-based catalysts, with proven performance in ethylene epoxidation. Unfortunately, these catalysts

cannot be used for propylene epoxidation because activation of the allylic hydrogen atoms in propylene result in total combustion of the substrate.[13,14] To solve this problem, the scientific community has dedicated significant efforts towards developing transition metal (Ag/Ni [15,16], Fe [17,18], Cu [19], among others) based catalyst with different oxidants (NO_2, O_2 and O_2/H_2). However, no catalysts with transition metals have reached acceptable selectivities compared to the benchmark Au/Ti-SiO_2 catalyst.

In this work, we present for the first time a Ni-based titanosilicate catalyst, which is very promising for the gas-phase catalytic epoxidation of propylene in terms of propylene conversion, PO selectivity and H_2 efficiency, with respect to Au-loaded catalysts. For comparison purposes, the catalytic performance will be compared with that of another transition metal-based catalysts (Fe), due the low cost of this transition metal and the resulting interest for the scientific community[17]. Furthermore, and since the vast majority of information found in the literature regarding the theoretical investigation of the epoxidation reaction refers to gold-based catalysts as the active phase, in this paper we have carried out a preliminary DFT study of the characteristics that make this nickel catalyst active and selective for propene epoxidation.

2.- MATERIALS AND METHODS

2.1.- Materials.

Titanium (IV) ethoxide (Sigma-Aldrich), tetramethyl orthosilicate (Sigma-Aldrich), nickel nitrate ($Ni(NO_3)_2 \cdot 6H_2O$, 99.99%, Sigma-Aldrich), iron nitrate ($Fe(NO_3)_2 \cdot 9H_2O$, 99.95%, Sigma-Aldrich), ruthenium chloride ($RuCl_3$, Sigma-Aldrich), Pluronic F-127 (Sigma-Aldrich), urea (99%, Merck), glacial acetic acid (HAc, 99%, Sigma-Aldrich), sodium hydroxide (NaOH, 99.99%,

Sigma-Aldrich) and deionized water were used in the present work. All reactants were used as received without further purification.

2.2.- Catalyst preparation.

2.2.1.- Synthesis of $Ti_{0.01}$-SiO_2. The mesoporous silica has been prepared adapting a synthetic protocol described elsewhere.[6,20] For the synthesis, 0.400 g of surfactant (Pluronic F-127), 0.452 g of urea, and 5.052 g of aqueous acetic acid (0.01 M) were mixed under vigorous stirring for 80 min, the final pH of the solution being around 4. Then the solution was cooled in an ice−water bath under continuous stirring and the previously mixed titania and silica precursors (titanium(IV) ethoxide and Tetramethyl orthosilicate, respectively) were added dropwise. This solution was kept under stirring for 40 min at 0°C. The sol was introduced in a teflon-lined autoclave. Then, the autoclave was heated at 40°C for 20 h to produce the aging of the sol (the pH after this step was around 4) followed by a hydrothermal treatment at 120°C for 6 h, to produce the urea decomposition (the final pH of the supernatant liquid was around 9−10). The final product was then calcined at 550ºC for 6 h (heating rate 3ºC/min).The BET surface area for the synthesized Ti-SiO_2 is 227 m^2/g.

2.2.2.- Transition metal impregnation. For the Ni impregnation, the necessary amount of $Ni(NO_3)_2 \cdot H_2O$ was dissolved in 20 ml of deionized water to prepare the catalysts with the different loadings. After dissolution, 1.0 g of Ti-SiO_2 were added to the solution. Then, a freshly prepared NaOH solution (2 M) was added dropwise until a pH of 10.5 was reached producing a color change from colourless to light green. The suspension was stirred at room temperature for 2 hours, filtered and washed with water until neutral pH was obtained in the filtration waters. Finally, the catalysts were dried at 100ºC before their use in the catalytic tests. Four different Ni loadings (wt. %) were

prepared: 0.5, 1, 2, and 5 wt. % Ni/Ti-SiO_2. For comparison purposes in terms of performance in the propylene epoxidation reaction, iron and ruthenium-based catalysts were also prepared. For these other transition metals, catalysts with 1 wt% loadings were prepared following the same procedure using the corresponding metal salts (see Experimental section).

2.3.- Characterization.

All the prepared catalysts have been characterized by Transmission Electron Microscopy (TEM) coupled to Energy Dispersive X-Ray Analysis (EDX) with a JEOL JEM-2010 microscope operating at 200 kV with a space resolution of 0.24 nm. TEM analyses allowed the evaluation of the metal species incorporation, the formation of small particles of metal and the quantification of the metal loading by the coupled EDX. Spectroscopic techniques were also used for characterization purposes. The prepared materials were analyzed using an Ultraviolet–Visible–Near-Infrared (UV–Visible–NIR, V-670, JASCO) equipped with a double monochromator system, a photomultiplier tube detector and an integrating sphere (ISN-723 UV–Visible–NIR, JASCO) which enables the possibility of measuring the diffuse reflectance or diffuse transmittance of a solid powder. In situ Fourier Transform Infrared Spectroscopy (FTIR, FTIR-4100, JASCO) was also used for the study of the solid-gas reaction in the different catalysts. The results have been presented by subtracting the spectrum corresponding to the pure catalyst to that obtained at the same temperature. Inductively coupled plasma-optical emission spectroscopy (ICP-OES), in a Perkin–Elmer Optima 4300 system was used to obtain the metal loading of the catalysts (Ni). The necessary amount of sample was dissolved in 0.1 ml of HF (5 vol.%) at room temperature, in order to ensure the total dissolution of the samples, and then diluted to the linear iron detection range (0.05–10 ppm). The electronic states were determined by X-ray Photoelectron Spectroscopy (XPS)

using a K-Alpha spectrometer from Thermo-Scientific, equipped with an Al anode. The X-Ray penetration depth for this equipment is between 2 and 3 nm under the operating conditions.

High-Resolution Transmission/Scanning Transmission Electron Microscopy, (S)TEM, studies were performed on a double aberration-corrected FEI Titan^3 Themis 60-300 microscope operated at 200 kV in High-Resolution TEM mode, additionally the microscope was operated at 80 kV to minimize sample damage effects for elemental mapping with energy dispersive X-ray spectrometry (XEDS) in STEM mode. This instrument is equipped with a monochromated, high brightness XFEG source and a high sensitivity, high efficiency Super-X EDS system, integrated by 4 window-less SDD detectors symmetrically arranged around the sample and the objective lens pole pieces.

The acquisition of XEDS maps was carried out using an electron probe less than 0.5 nm, beam current of 60-70 pA, convergence angle of 19 mrad and 20 keV of range. Each chemical map was collected as a series of frames, where the same region, typically 350 x 350 pixels, was scanned 50 times, employing a spatially drift-compensation tool, with a dwell time per pixel of 100 μs, taking approximately 10-12 minutes per spectral image dataset. STEM-HAADF images were recorded under analogous conditions employing an annular dark field detector with a collection range of 50 -200 mrad.

HRTEM images were analyzed in reciprocal space by measuring on the corresponding Digital Diffraction Patterns (DDPs) using Velox and Gatan Digital Micrograph (DM) software. Resolution in the order of 0.12 nm is achieved under the employed low voltage operating conditions. In addition, Eje-Z program[21] was used for the interpretation of HRTEM images and modeling the possible nickel phases present in the samples.

The XEDS- spectrum image post-treatment data was performed using Velox software, which allows quantification by Cliff-Lorimer (K-factor) method including absorption correction. The elemental maps of Silicon, Titanium and Nickel, were generated using the family of the Si-Kα, Ti-Kα and Ni-Kα lines at 1.74, 4.51 and 7.47 keV respectively.

The electron microscopy samples were performed by directly depositing a portion of the fine powder of the catalyst samples onto holey-carbon coated Cu grids, to avoid any contamination due to the use of solvents.

2.4.- Propylene epoxidation test.

Prior to the catalytic tests, all catalysts were pre-treated up to 500ºC (10ºC/min) with 5 vol. % H_2 in He to reduce the formed $Ni(OH)_2$ nanoparticles. The catalysts were tested for at least 4 h under steady-state conditions at 200ºC. The standard conditions were WHSV of 10,000 $ml \cdot g^{-1} \cdot h^{-1}$ and a gas stream composed of 10% C_3H_6, 10% H_2, 10% O_2 in 70% He was used in the catalytic tests. The outlet gas composition was analyzed with a MS (Pfeiffer Vacuum, Thermostar) and a GC chromatograph (Agilent 7820A) equipped with two columns, PoraBond Q (Agilent) and CTR-I (Alltech), for the separation of the organic (propylene, propane, propylene oxide, acetaldehyde, acetone) and the inorganic (mainly, O_2 and CO_2) compounds respectively. Propylene conversion, PO yield, PO selectivity and H_2 efficiency were determined and calculated in all catalytic tests following the previously published equations [22]. The hydrogen efficiency was obtained taking into account all the possible reactions that may lead to the different reaction products, including the formation of water from H_2 and O_2. All parts of the reaction system were heated to avoid water condensation. The gas flow rate of the reaction stream was measured for all experiments at the inlet and outlet of the reactor before and during the reaction. Since all the reactants and products,

except for water, were precisely measured, as well as the gas flow rate, the mass balance allowed us to calculate the hydrogen efficiency.

$$\text{Propylene Conversion (\%)} = \frac{C_{C_3H_6-\text{in}} - C_{C_3H_6-\text{out}}}{C_{C_3H_6-\text{in}}} \times 100$$

$$\text{PO Yield (\%)} = \frac{C_{\text{PO - out}}}{C_{C_3H_6-\text{in}}} \times 100$$

$$\text{PO Selectivity (\%)} = \frac{C_{\text{PO - out}}}{C_{C_3H_6-\text{in}} - C_{C_3H_6-\text{out}}} \times 100$$

$$H_2\text{Efficiency (\%)} = \frac{C_{\text{PO - out}}}{C_{H_2O-\text{out}}} \times 100$$

2.5.- Computational details.

DFT calculations were conducted by means of the CP2K package code in its 4.1 version using the QUICKSTEP module.[23] Dispersion corrected (D3)[24] GGA-PBE [25] exchange correlation functional under periodic boundary conditions (PBC) were used for all simulations. During geometry optimizations all the system was allowed to relax to find its local minimum. Adsorption energies were calculated by using the equation:

$$E_{ads} = E_{slab/molecule} - (E_{slab}+E_{molecule})$$

Additional information on computational details can be found in the supplementary information document.

3.- RESULTS AND DISCUSION.

3.1.- Characterization of the catalysts

The Ti-SiO_2 catalyst support was first characterized by HR-STEM HAADF and HR-STEM-XEDS (Figure 1). STEM-XEDS elemental maps showed that Ti was highly dispersed, mixed at atomic level with Si in the support, as shown in Figure 1(b). Quantification of the elemental maps indicated in this case a Ti content slightly below the average composition, 0.8% at. As expected, other areas with higher Ti contents were also detected, as shown in Figure S1 in Supporting Information. In all cases, Ti was found well dispersed in the SiO_2 matrix. No evidence of separate TiO_2-like areas could be detected.

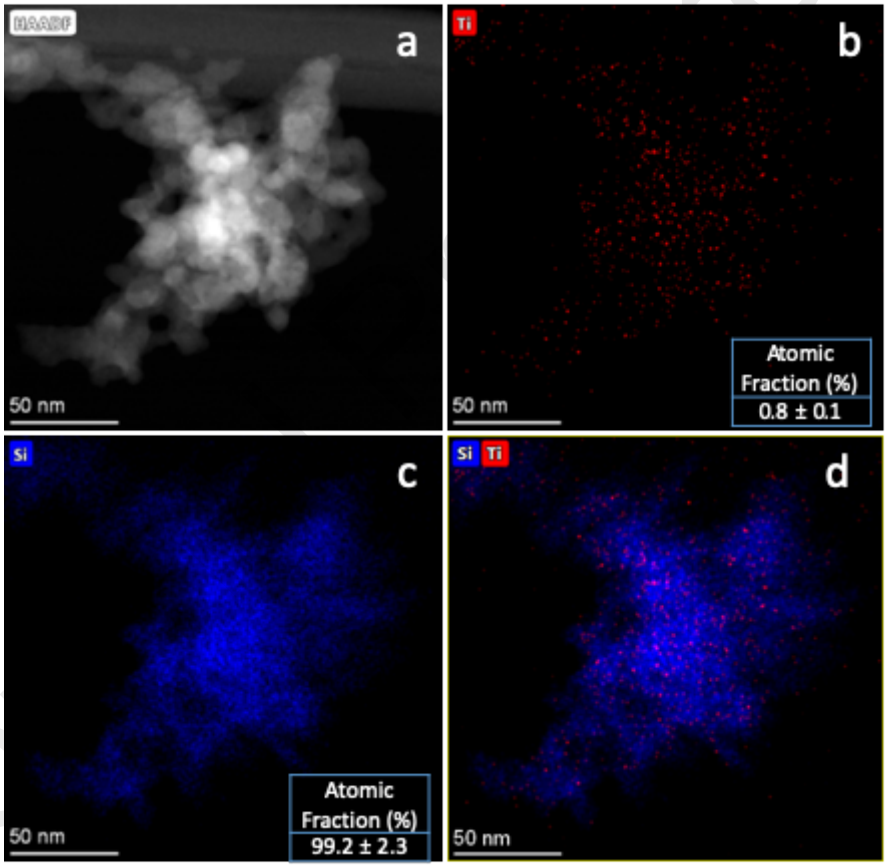

Figure 1. (a) Representative STEM-HAADF image of the Ti-SiO_2 support; (b-d) Ti, Si and overlaid maps obtained by STEM-XEDS.

Moreover, as shown in Figure 2, HRTEM images indicated that the support was formed by nanosized amorphous aggregates, Figure 2(a). Additional HRTEM images, including Digital diffractograms (DDPs) depicting the amorphous structure of the support have been gathered in Figure S2. No evidence of crystalline areas could be obtained in the HRTEM study of the support.

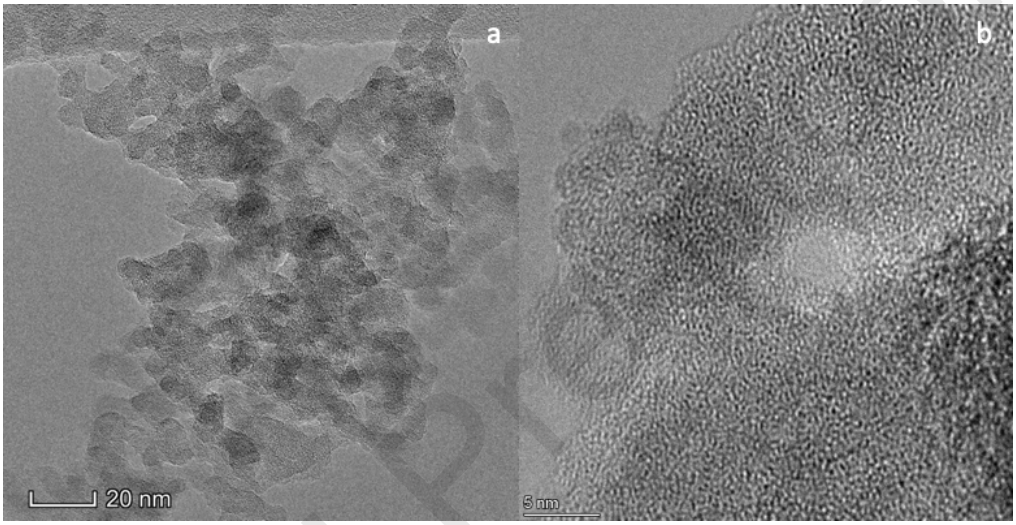

Figure 2. Representative medium (a) and high (b) magnification HRTEM images of the Ti-SiO_2 support.

The transition metal-based catalysts were synthesized by controlled precipitation of $Ni(OH)_2$ in basic media (see Experimental section), on the surface of Ti-SiO_2. This support was prepared by one-step procedure following a well-known methodology [20]. All catalysts prepared in this work were characterized with ICP-OES, in order to determine the metal loading. In all cases, the real Ni and Fe loadings were very close to their respective nominal loadings. UV–Vis absorption is a characterization technique very useful to study of the incorporation of Ti into the silica framework.[26] The UV-Vis analysis revealed that Ti is incorporated as single sites into the silica

framework mainly in tetrahedral coordination even though a small fraction of Ti in octahedral coordination is obtained in all samples (Figure 3).[20] As an example, a slight increase of the absorption about 380 nm is observed after the incorporation the Ni in the catalysts, in all cases (Figure 3). This band further increases after the reduction pretreatment of the Ni NPs indicating the presence of Ni^0 in the catalyst. The increase of the band at 380 nm is accompanied by a broadening of the band at 220 nm, which may indicate that a small fraction of the tetrahedrally coordinated Ti adopts an octahedral coordination after the reductive pretreatment.

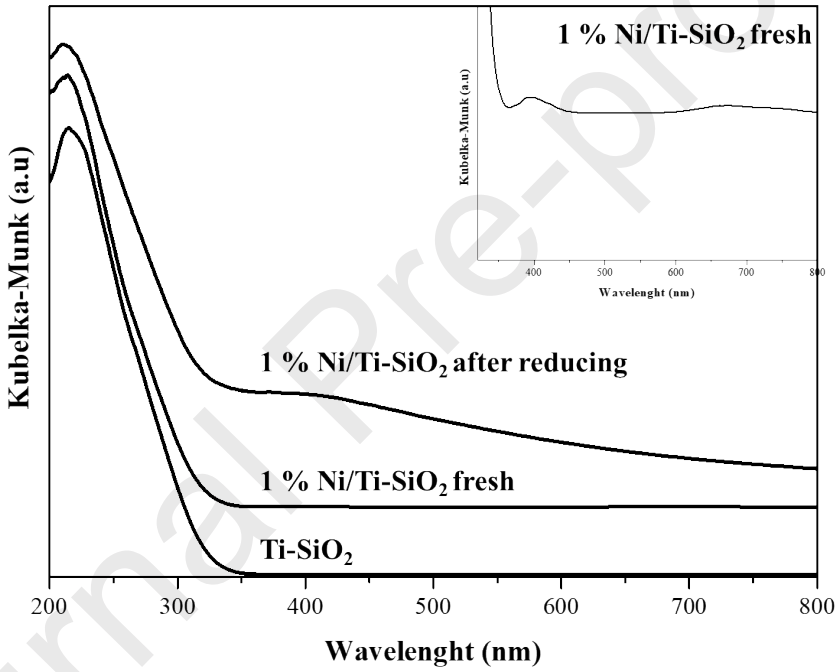

Figure 3. Solid UV–Vis reflectance spectra (presented in Kubelka-Munk units) for the raw Ti-SiO_2 and 1% Ni/Ti-SiO_2 fresh and after reducing. Inset: Magnified view of 400-800 nm region for sample 1% Ni/Ti-SiO_2 showing a small band at 380 nm.

TEM characterization (Figure 4) shows a really good dispersion of the metal for the Ni-based catalysts for loadings between 0.5 and 1 wt. % Ni/ Ti-SiO_2. On the other hand, for 2 and 5 wt. %

Ni catalysts, a more distinct presence of the Ni particles can be observed due to the high metal loading (Figure 4). The EDX analysis confirmed the presence of the metal in all cases.

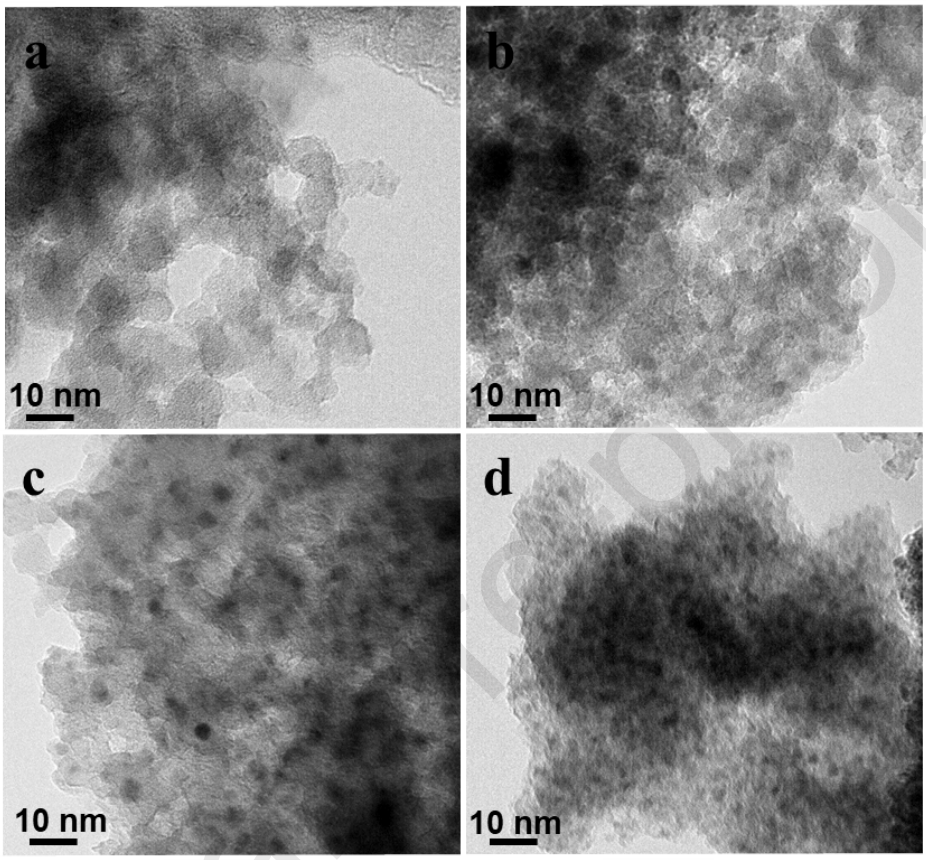

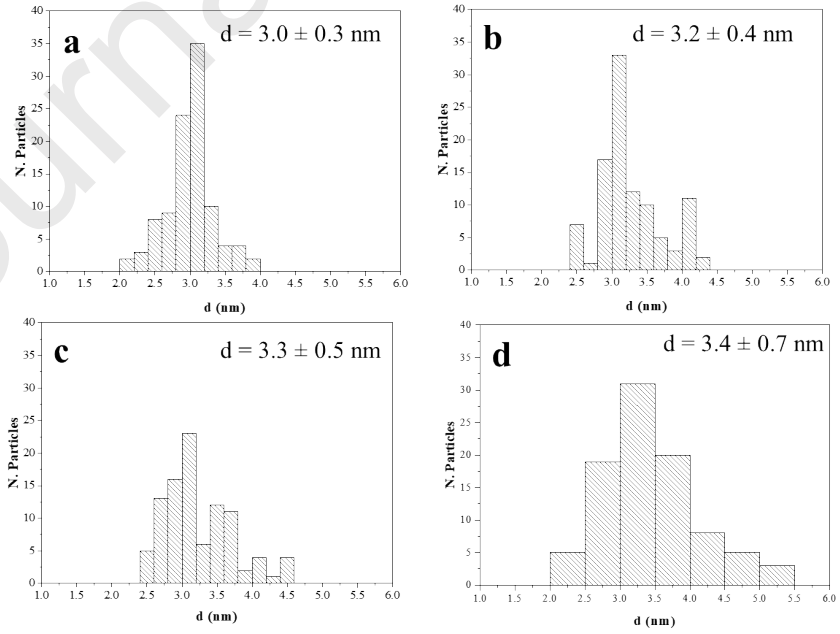

Figure 4. TEM images of (a) 0.5 % Ni/Ti-SiO_2, (b) 1 % Ni/Ti-SiO_2, (c) 2 % Ni/Ti-SiO_2, (d) 5 % Ni/Ti-SiO_2 and their corresponding histograms.

The STEM-XEDS analytical investigation of the fresh 0.5% Ni loaded catalyst, Figures 5(a-e), showed that the metal was finely dispersed over the surface of the support, in good contact with the underlying Ti areas. Figure S3 provides additional examples.

HRTEM images allowed detecting the presence of Ni in this catalyst in the form of 1.5-3.5 nm NiO particles, Figure 6. Characteristic fringe patterns of Ni were also observed in some particles (see Figure S4) most likely due to reduction of the small NiO particles under the electron beam.

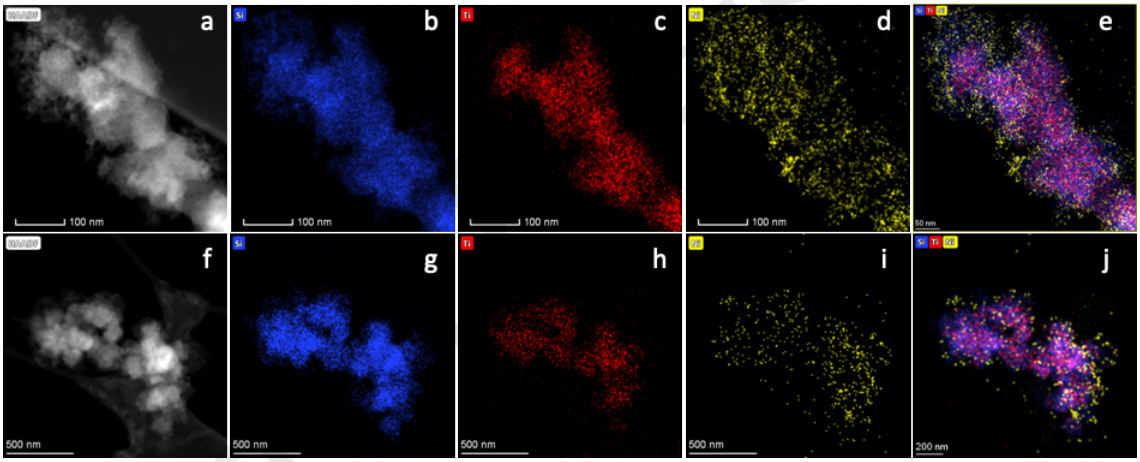

Figure 5. HR STEM-XEDS analytical study of the 0.5% Ni/Ti-SiO_2 catalyst as prepared (upper row) and after reaction (bottom row). STEM-HAADF (a,f), Si (b,g), Ti (c,h), Ni (d,i) and overlaid (e,j) maps are included.

No significant change was detected in the nanostructure of the 0.5% Ni/Ti-SiO_2 catalyst after reaction, either in terms of the spatial distribution of the different elements present in the catalyst, as revealed by STEM-XEDS, Figure 5(f-j), or in the nature of the supported Ni phase, Figure 6(d).

Only a small increase in the size of these particles, now closer in average to 3 nm, could be observed.

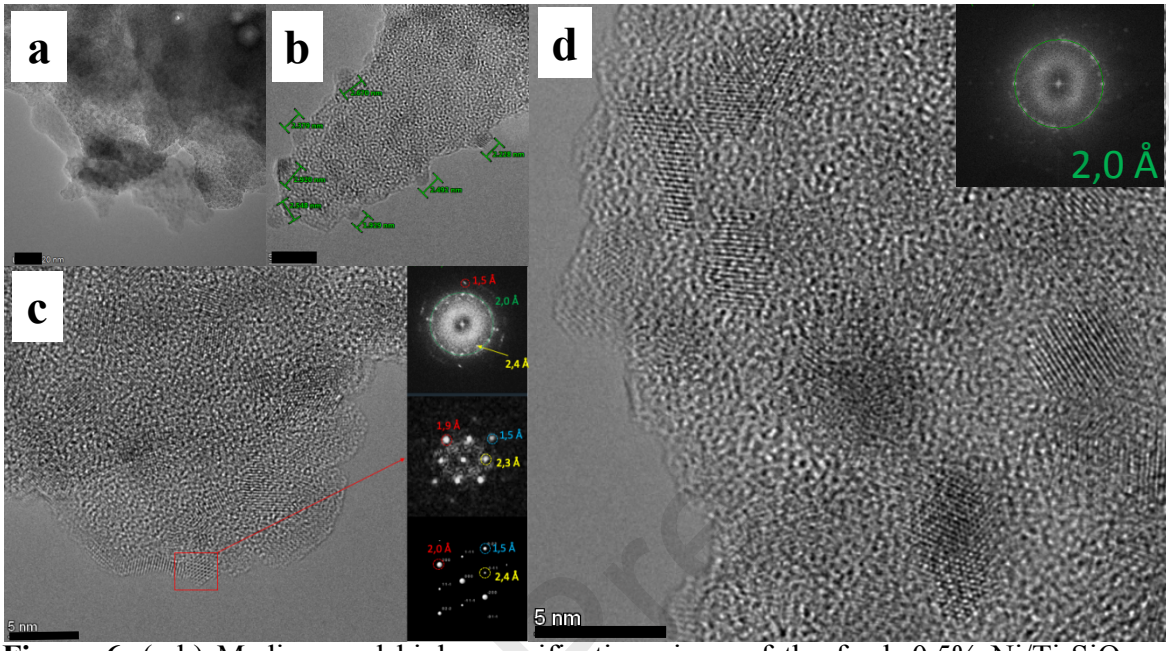

Figure 6. (a-b) Medium and high magnification views of the fresh 0.5% Ni/Ti-SiO_2 catalyst. Different nanosized particles are marked in (b); (c) HRTEM view of the fresh catalysts where the structure of the particles is revealed. A DDP from the whole area (top-right inset), showing the 0.24 nm reflections characteristic of NiO is included. The DDP at the middle corresponds to a NiO down the [110] zone axis. A simulated DDP of NiO down [110] is shown at the bottom for comparison; (d) representative HRTEM image of the 0.5% Ni/Ti-SiO_2 catalyst after reaction. A DDP showing a 0.2 nm reflection ring characteristic of Ni is included as inset. Scale bar for Figure 6(a): 20 nm; Scale bars for Figures 6(b)-(d): 5 nm.

The fresh catalysts with the highest Ni loading was also analyzed in detail by HR(S)TEM. In this case STEM-XEDS results, Figure 7(a-e), showed a rather uniform and nearly complete

coverage of the support particle surfaces by the metallic phase, as expected from the large increase in metal loading. HRTEM images (Figure 8) showed once again a system of nanosized Ni-containing particles which eventually form long units which decorate in a continuous-like way the surface of the support particles, as marked with deep blue arrows in Figure 8 (a,c). The analysis of the lattice fringes revealed the presence of both NiO and Ni, as in the low loading catalyst.

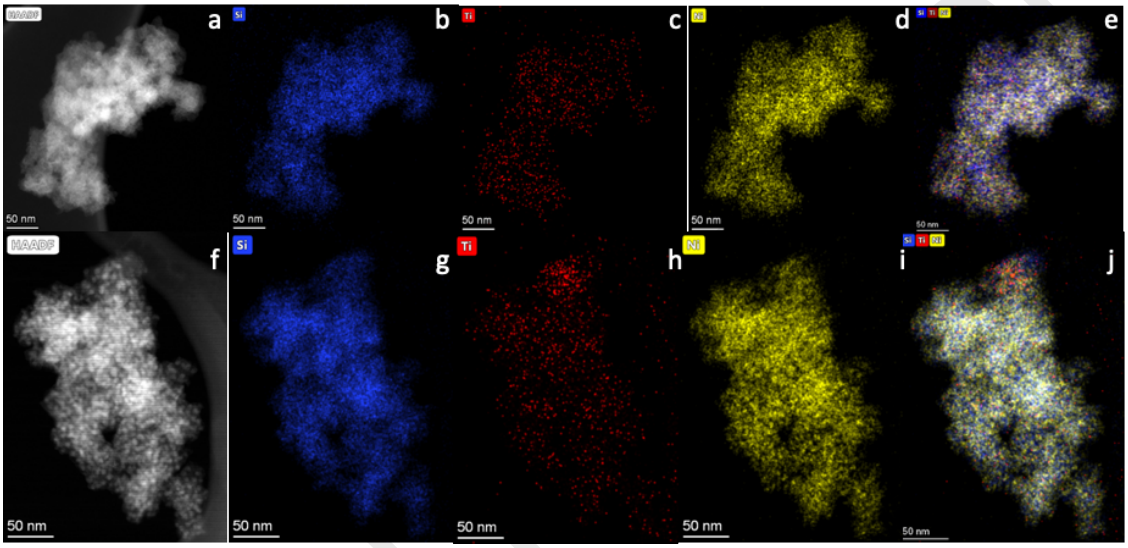

Figure 7. HR STEM-XEDS analytical study of the 5% Ni/Ti-SiO_2 catalyst as prepared (upper row) and after reaction (bottom row). STEM-HAADF (a,f), Si (b,g), Ti (c,h), Ni (d,i) and overlaid (e,j) maps are included.

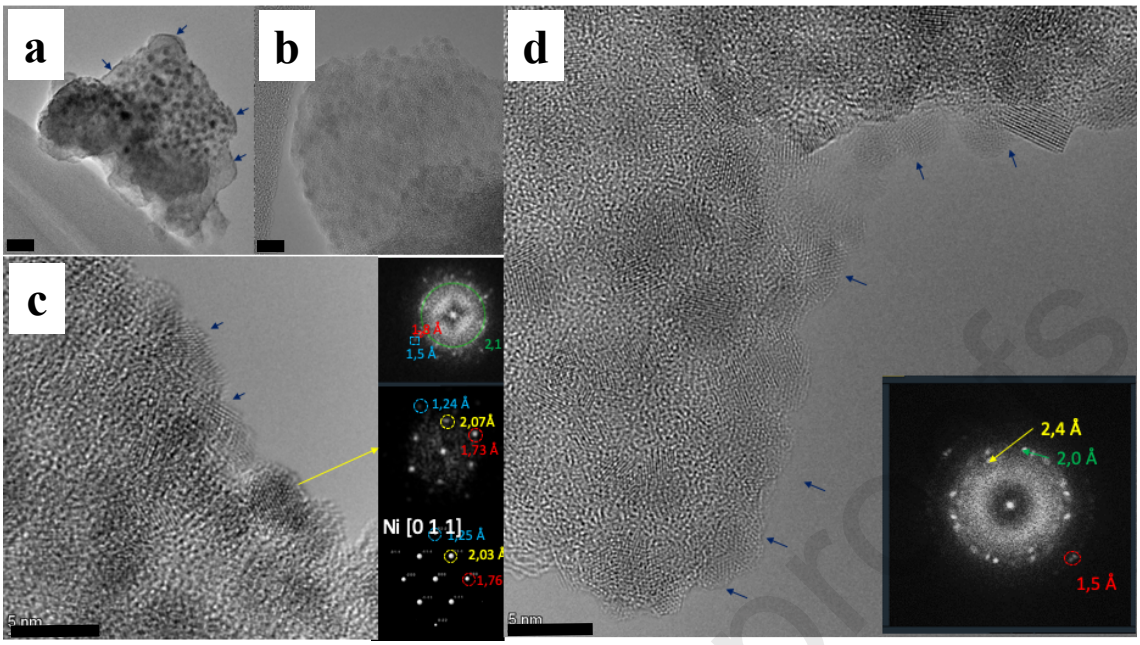

Figure 8. (a-b) Medium and high magnification views of the fresh 5% Ni/Ti-SiO_2 catalyst. Deep blue arrows point to areas where a nearly continuous coverage of the support by Ni particles is observed. Individual nanosized particles are clearly observed in (b); (c) HRTEM view of the fresh catalysts where the structure of the particles is revealed. A DDPs from the whole area (top inset), showing the different reflections characteristic of Ni. The DDP at the middle corresponds to a Ni particle along the [110] zone axis. The DDP at the bottom corresponds to a simulated DDP for Ni along the [110] axis; (d) representative HRTEM image of the 5% Ni/Ti-SiO_2 catalyst after reaction. A DDP of the whole area showing different NiO reflections is included as inset. Scale bar for Figure 8(a): 20 nm; Scale bars for Figures 8(b)-(d): 5 nm.

As in the case of the lowest loading catalyst, the major nanostructural features of the 5% Ni/Ti-SiO_2 catalysts did not significantly modify after reaction, as shown in Figures 7(f-j), 8(d) and S5. Nevertheless, it must be mentioned that some degree of Ni particle agglomeration is observed, as

shown in Figures 7(f) and S5(f). As with the catalyst, with a low Ni loading, fringe patterns characteristic of Ni was also observed in some particles (Figure S6)

Ni and Ti XPS analysis offered information about the different Ni and Ti species present on the surface for the catalysts (see Figure 9 and S7). Ni 2p binding energy presents some interesting data for nickel catalysts supported on titanosilicates materials. The fresh sample with 1 wt. % Ni/ Ti-SiO_2 (without pretreatment) does not present a band at a binding energy of 852.8 eV characteristic of zerovalent nickel. However, the sample with 1 wt. % Ni/Ti-SiO_2 pretreated in H_2 at 500 ºC has the characteristic band of Ni^0 (Figure 9). This fact indicates the reduction of the $Ni(OH)_2$ species (band at 856.7 eV) supported on the titanosilicate to metallic species (Ni^0).[27,28] Moreover, the presence of Ni species on the surface of titanosilicate shifted the Ti $2p_{3/2}$ BE signal from 460.48 eV (in the support) to 459.3 eV (after Ni loading) (Figure S1), indicating the existence of Ni species with a strong interaction with Ti species [29], which suggests the formation of Ti-O-Ni species. The presence of metallic particles (Ni) on the support has a relevant effect in the catalytic properties of the catalyst as it has been described in the literature[8] and below in this work. The XPS spectrum collected after reaction showed that the Ni species supported on the catalyst come back to the oxidized species given that the post-reaction sample did not show the characteristic band of Ni^0 at 852.8 eV (Figure 9). The same XPS analyses were also performed in the 0.5 wt. % and 5 wt. % Ni/ Ti-SiO_2 and the results obtained (not shown) were very similar to those shown in Figure 9.

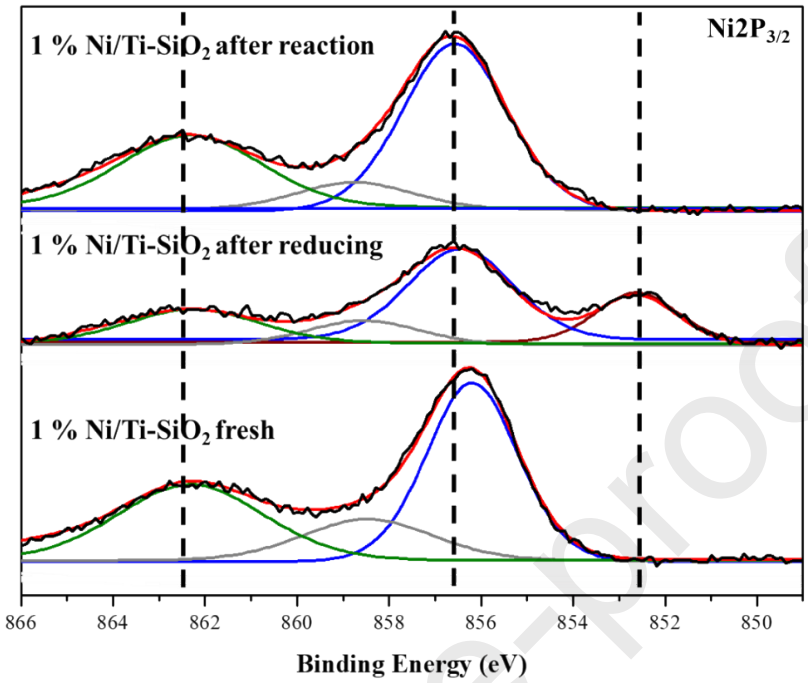

Figure 9. $Ni2P_{3/2}$ XPS spectra of the raw 1% $Ni/Ti\text{-}SiO_2$, 1% $Ni/Ti\text{-}SiO_2$ after reduction and $Ni/Ti\text{-}SiO_2$ after reaction.

3.2.- Propylene epoxidation reaction

The catalytic results under steady-state conditions for the gas-phase propylene epoxidation reaction at 200ºC for all the catalysts prepared in this work are shown in Table 1. This temperature was found to be the best for the gas-phase propylene epoxidation reaction using the Ni-based catalysts as shown in Table S1, and thus this was also the temperature of choice to test all transition metal-based catalysts. An increase in the reaction temperature can favor the sintering of the Ni nanoparticles, thus having a negative impact on the catalytic activity and selectivity. The results of the $Ti\text{-}SiO_2$ and Ni/SiO_2 samples in the catalytic test are not presented in Table 1 because these catalysts did not present any catalytic activity for this reaction. This clearly shows that both well-

dispersed Ni and Ti species with a strong interaction are needed in the catalysts to obtain suitable PO generation values in the presence of H_2/O_2 mixtures. Table 1 shows that all Ni catalysts present a conversion of propylene below 10% irrespective of the metal loading at 200ºC under steady-state conditions after the reduction treatment. It must be noted that all catalysts showed a stable catalytic performance once the steady state was reached. Throughout each epoxidation reaction (which, as mentioned in the experimental section lasted 4 hours) the variation in activity or selectivity was always below 5% (see Fig. S8).

The Ni-based catalysts have similar propylene conversion compared to Au-based catalysts (e.g. Au supported on Ti-SiO_2) described in the literature (Table 1). Addressing the selectivity towards PO, the catalysts with low Ni loading (0.5% and 1%) present an excellent PO selectivity of around 90%. However, higher loadings of Ni on the surface of the titanosilicate decreased the selectivity towards PO as reported for the catalysts based on Au. This effect could be due to the different loadings of the catalysts (this is clearly shown by comparing Figures 5 and 7). As a result, high amounts of Ni in the catalyst may block the Ti single site species on the surface of the support. As a result, these catalysts are not efficient in the propylene oxide generation due to a blocking of the active site, as we will discuss below. It must be noted that a similar active site engineering has been recently reported by Hutchings et al., in which they state that a suitable thermal treatment followed by reduction at 450ºC is essential for the development of peripheral Pt/TiO_2 sites, which are "most likely active sites" in the selective hydrogenation of 3-nitrostyrene. With respect to H_2 efficiency, an increase in the loading of Ni on the surface of the support causes a drop in this parameter. These results show the outstanding performance of the catalysts with low (0.5 wt. and 1% wt.) Ni loadings for this reaction. These catalysts present the best dispersion of nickel and

titanium species on and into the silica (see Figure 4) which results in excellent catalytic properties with respect to other catalysts with higher amounts of Ni (2 wt. % and 5 wt. % Ni/ Ti-SiO_2).

Moreover, these catalysts (0.5 wt. % and 1 wt. % Ni/ Ti-SiO_2) show similar catalytic properties than Au-based catalysts (7% of C_3H_6 Conversion and 90 % of PO Selectivity) being the catalyst based on Au the most attractive for this reaction reported in the literature.[6,7] In this aspect, the catalysts described in this work present similar catalytic performance, but using a significantly cheaper non-noble metal thus being more cost-effective than the catalyst based on gold. Another important factor is that the PO formation rate for the best Ni-based catalyst described in this work is 112 g PO/(kg_{cat}·h), similar to the benchmark Au-based catalysts described in the literature (116 g PO/(kg_{cat}·h)).[31] This result of PO formation rate makes the nickel-based catalysts described in this work a competitive candidate for their use in the production of propylene oxide at an industrial scale. In this respect, the most promising catalysts were recovered and reused for at least three catalytic cycles, displaying no significant loss of performance after each cycle.

The Ni/Ti atomic ratios calculated for the catalysts in the order 0.5-1-2-5 wt.% are 0.51, 1.02, 2.04, and 5.11, respectively. Although it is very difficult to determine how many Ti atoms are covered by Ni, we have done an estimation as follows. We calculated the percentage of support surface area covered by the Ni NPs on the Ti-SiO_2 assuming that Ni is in its zerovalent state and the NPs are in semispherical form. The values obtained were 0.48, 0.96, 1.91 and 4.78 % for the samples with a loading of 0.5-1-2-5wt.%, respectively. Assuming that Ti is homogeneously distributed in the Ti-SiO_2 the percentage of surface area corresponding to the Ti species would be around 1%. Since Ni distribution on the support surface is favored near Ti species (see XPS results and Section 3.3), the results show that the number of Ti atoms covered by Ni would be high for the sample with a 5wt% Ni. This is in very good agreement with the observed catalytic results.

Table 1 also presents the data obtained using the Fe-impregnated catalyst. It is clear that the two catalysts perform very poorly in this reaction. In the case of the Fe-based catalyst, apart from a very low propene conversion, the most noticeable result was that the predominant reaction was the complete oxidation of propene to CO_2 and water, which is consistent with literature data, which indicate that Fe is too acidic and thus promotes the abstraction of the allylic hydrogen of propylene, favoring its complete oxidation[17,18]. For the sake of comparison, and despite not being economically competitive to 3d transition metals, a Ru catalyst (prepared in the same way as that reported in our study, see Table 1) was also tested. While the conversion increased significantly over the Fe-based catalyst, the selectivity towards the desired product was very low, with propane, isopropanol and acetaldehyde being predominant over propylene oxide. In this respect, the Ni/Ti-SiO_2 catalysts possesses the optimum interplay between oxygen and propylene activation, with very high selectivity (over 90%) towards the desired product.

Table 1. Catalytic results under steady-state for the gas-phase propylene epoxidation reaction at 200ºC.

Catalyst	C_3H_6 Conversion (%)	PO Yield (%)	H_2 Efficiency (%)	PO Selectivity (%)	Others Selectivity[a] (%)	CO_2 Selectivity (%)
0.5 % Ni/Ti-SiO_2	6.3	5.4	36.9	85.5	4.5	10
1 % Ni/Ti-SiO_2	7.5	6.9	16.3	90.7	6.3	3
2 % Ni/Ti-SiO_2	5.8	3.0	10.6	52.2	6.7	41
5 % Ni/Ti-SiO_2	9.3	1.4	1.5	14.4	9.6	76
0.05Au/TS-1[31]	8.8	n/d	n/d	81	14.7	4.4
1% Fe/Ti-SiO_2	1.1	<0.1	n/d	3	<1	~96
1% Ru/Ti-SiO_2	4.7	<0.1	1	2	~10	~88

[a] Propane, Acetone and Acetaldehyde are the main organic by-products obtained in the catalytic

reaction for Ni-based catalysts. Propanal, acrolein, and propanol were not detected in any of the experimental runs.

In order to clarify the performance during reaction for the best catalyst, FTIR measurements before and after the reaction with the 1 wt. % Ni/ Ti-SiO_2 catalyst were carried out to investigate the surface species formed during reaction (see Figure 10). In the fresh catalyst (1 wt. % Ni/ Ti-SiO_2) no bands were observed at 2980, 2939 and 2880 cm^{-1}. These bands are assigned to the C–H stretching vibrations of bidentate propoxy species. After reaction these bands appear, which can result from PO adsorption on Ti sites.[8] This is also observed in the Au based catalysts indicating that the performance of these two catalysts converting propylene into propylene oxide may be similar.[8,12] In this respect, it would appear that the Ni species located near tetrahedral Ti would be performing the same role as Au nanoparticles in the benchmark catalyst. In this respect, the DFT results obtained in this study (vide infra) imply that the active sites are the interfaces between the nickel particles and the tetrahedral Ti of the support, which, as evidenced from our catalytic data together with the FTIR experiments, perform similarly to the benchmark Au-based catalyst, suggesting the possibility that both catalysts follow a similar reaction mechanism to produce propylene oxide.

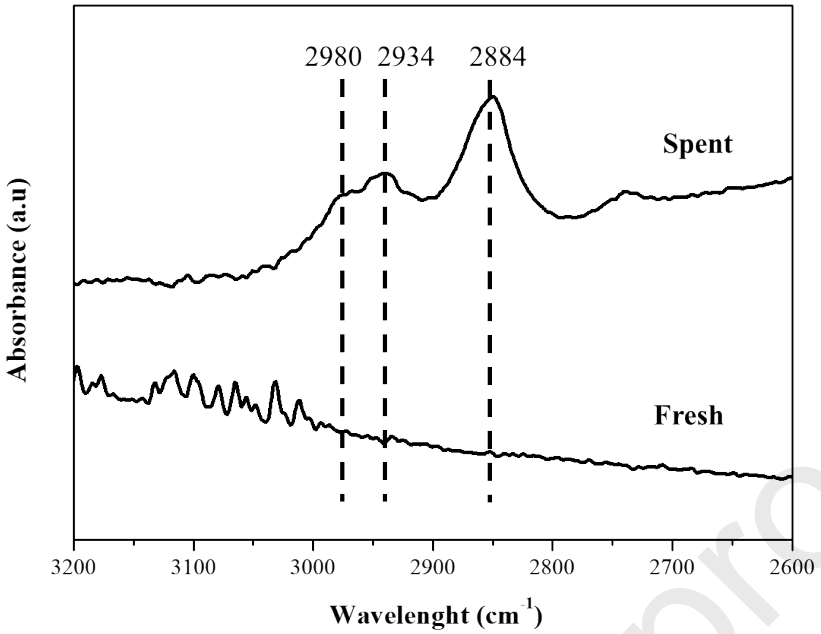

Figure 10. FTIR spectra of the fresh and the spent 1 wt. % Ni/ Ti-SiO_2 catalyst.

3.3.- Computational study

The majority of theoretical chemistry papers found in the literature are focused on the study of TS-1 and Au/TiO_2 catalysts.[32-34] It is known that one of the characteristics of Au as active phase is its low capacity to promote catalytic reactions compared to other transition metals. Specifically, the capacity that gold possesses for chemical oxygen chemisorption is limited.[35-37] Special conditions are needed in the structure of the gold particle (clusters with odd number of atoms, flexible geometries, alloys, hydrogen pre-chemisorption)[10] to activate the oxygen molecule for further reaction.

It is precisely this low ability to activate reactive molecules, which has made gold-based catalysts effective in reactions in which selectivity prevails over total catalytic activity [35,38] such as the propylene epoxidation reaction. The use of more reactive metal phases in the epoxidation reaction

usually promotes the total oxidation of the hydrocarbon to carbon dioxide and the hydrogen to water (as is the case of the Fe-based catalyst[17,22] used in this study, see Table 1).

However, the results presented in this article show that the epoxidation reaction can be carried out with high selectivity using nickel as metal phase. Then, here we present a preliminary theoretical DFT study to try to understand the role of Ni species.

3.3.1.- Description of the computational system

The molecular system used is based in an amorphous SiO_2 model. Specifically, a model of a MCM-41 wall silica structure presented in this work [39] has been modified and adapted as support for our catalyst model (424 atoms per unit cell). In the model used (Figure 11), one surface silanol has been replaced by Ti-OH group leading to a Ti tetrahedral single site placed in the silica framework, as it was deduced from the solid UV-Vis experiments. Some authors [32,40] demonstrated that tetrahedral Ti-OH are the active species to produce hydroperoxide intermediates (Ti-OOH) that is one of key intermediates in the epoxidation reaction. It is also expected that this titanium site would be more accessible to reactants than non-hydroxylated titanium.

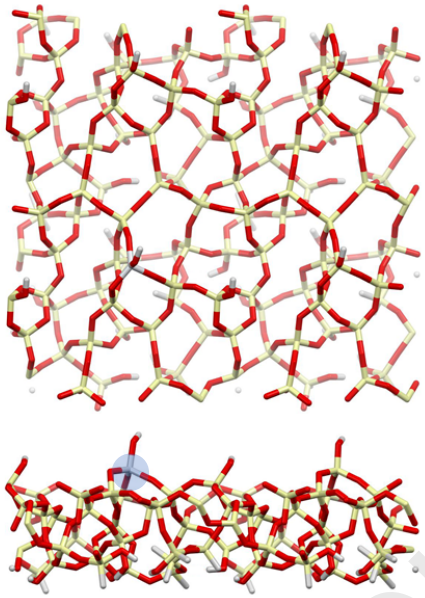

Figure 11. Top view and side view of the silica structure with intercalated Ti atom (Light blue circle in the lower diagram) in a Ti-OH site.

Our TEM results conclude that the catalyst is comprised of very small nickel particles (1.5-3.5nm) for the low metal content catalysts (0.5wt.%) as well as for the other catalysts. Thus, after optimization of the Ti/SiO_2 structure, a 10 atoms nickel particle (approx. 0.5 nm in diameter) has been added to the silica surface close to the titanium site and the geometry of the full structure was optimized. From our observations the Ni-Ti interface, where the epoxidation reaction is taking place (see below), is well represented in this model. Figure 12 shows a detail of the interface between the nickel particle and the Ti/SiO_2 structure. It can be observed that nickel presents a strong interaction with the silica surface. This behavior is observed in the displacement of the oxygen atoms of silica structure in contact with the metal interface (marked in yellow). In order to correlate these observations with our experimental data, the close interaction taking place between Ni and Ti forming Ni-O-Ti species, may be established during impregnation. Since Ti is significantly less electronegative than Si, the oxygen atoms located near the single-site Ti will bear

a larger (i.e. more negative) electron density, which may interact more favorably with the cationic Ni species which are present in the reaction medium in the initial steps of the impregnation procedure. Further precipitation of $Ni(OH)_2$ using NaOH would result in the clusters located in the vicinity of the single-site Ti which we have simulated in our work.

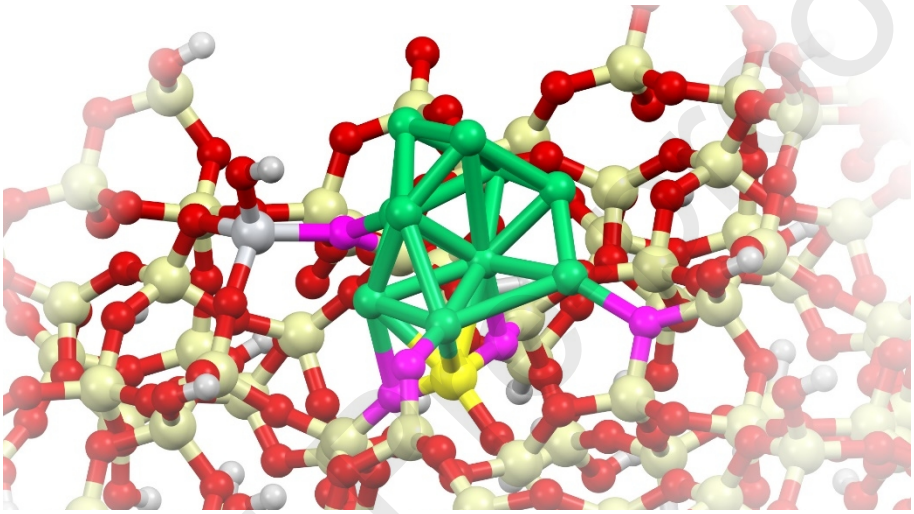

Figure 12. Detail of the interaction of the nickel particle with the Ti/SiO_2 framework. The distortion of the silica structure can be seen in the atoms marked in purple (oxygen) and in bright yellow (silicon).

3.3.2.- Molecular interaction study

To understand the interaction of the reactive molecules with the model system, several geometry optimizations with H_2, O_2, and C_3H_6 have been carried out and the adsorption energies have been calculated. Different departure geometries have been studied to ensure that a representative energy potential space with different local minimum is sampled. Also, for comparative purposes, the

optimization of some molecular adsorption geometries with the Ti/SiO_2 structure without nickel atoms was also calculated.

3.3.2.1.- Interaction with H_2 and C_3H_6

The interaction of H_2 with the system occurs mainly through the adsorption and dissociation of the hydrogen molecule over the nickel particle. The energies obtained in several attempts of chemisorbing H_2 on nickel atoms range between -0,9 and -1.2 eV. Different configurations have been studied with the adsorbed hydrogen on top, bridge and in hole positions and the values are in the order of the chemisorption energies obtained using Ni(111) as metallic surface.[41] The interaction of H_2 with the system without nickel leads to a low energy value typical of physisorption processes.

In the case of propylene, also several optimizations have been carried out with different starting geometries. The approximation of the olefin to the Ti site does not produce an optimized state with high adsorption energies: -0.05eV for the system without nickel, and -0.22 eV to the system with the nickel particle. However, the adsorption on the nickel atoms produces a strong interaction with an adsorption energy up to -2.02 eV. The carbon double bond length increases from 1.34 to 1.40Å indicating the activation of the molecule in the vicinity of nickel. However, this activation is far from the interface between nickel and Ti site, so an optimization approach with the propene close to the interface has been carried out. In this optimization, the molecule is less activated than in the previous case. However, an adsorption energy of -0.92 eV indicates that some activation is taking place and it may be sufficient to facilitate the formation of propylene oxide. For comparison purposes, Driscoll et al. [42] found adsorption energies between -0.4 and -0.6 eV approximately for an active Au/TiO_2 catalyst.

3.3.2.2.- Interaction with oxygen

One of the key aspects in the epoxidation process, is the interaction of the oxygen molecule with the active phase. Firstly, the direct interaction of oxygen with the Ti/SiO_2 surface (without nickel) leads to a weak adsorption. Only a physisorption-like behavior and energies have been achieved after different attempts in geometry optimization.

The oxygen adsorption simulations show that the nickel nanoparticle used in the system has a strong interaction with molecular oxygen. Two different optimizations have been done with different starting departure geometries. Figure 13 shows the final atom positions. Oxygen was adsorbed over two different zones of the nickel particle: far from Ti site (geometry I), and close to Ti site (geometry II). Adsorption energies are shown also in Figure 13.

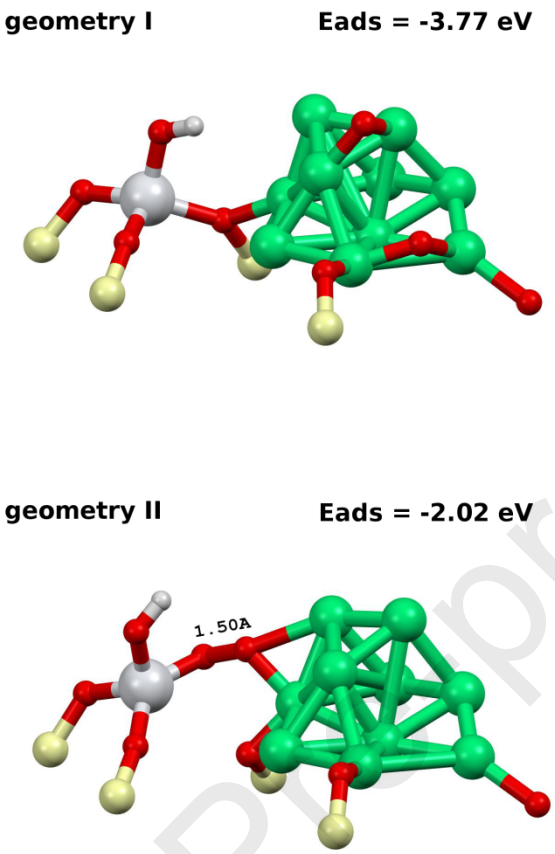

Figure 13. Detail of the two final geometries obtained during the adsorption of oxygen. Adsorption energies are also shown in eV.

The dissociation of the molecular oxygen during its adsorption on nickel that occurs in the geometry I takes place without any apparent activation barrier. A high adsorption energy (-3.77 eV) has been achieved. This dissociated atomic oxygen is more able to promote the oxidation of chemisorbed H_2 having a strong effect on the selectivity of the epoxidation reaction.[43] Furthermore, the absence of dissociation energy plus the higher adsorption energies obtained, implies that the metallic chemisorption sites available would be, practically, occupied with oxygen atoms, instead of hydrogen or hydrocarbon intermediates. That is why it is expected that during

the epoxidation reaction, the nickel particles would be superficially oxidized. This catalytic behavior is in agreement with the XPS results obtained in Figure 9, in which the spent catalysts show an oxidized nickel surface.

The geometry II in Figure 13 shows that, when an oxygen molecule is placed in the space between the Ti site and the nickel particle a synergistic co-adsorption of the molecule occurs. The O-O bond length increases from 1.23Å in molecular oxygen to 1.50Å that corresponds to a bond distance typical of peroxide species (H_2O_2 has a bond distance of 1.54Å). The previous geometry is a structure in which the total dissociation of the O_2 molecule has not been carried out. Thus, it could be an intermediate whose reactivity towards the total oxidation of H_2 or the hydrocarbon could be limited. In addition, the adsorption energy is lower than in the previous case, so it would be a more suitable species to be an intermediate in epoxidation reaction. [33,40]

To illustrate this, during the formation of this peroxide structure, a cleavage of one of the Ti-O bonds is proposed. Then, another free nickel atom participates in this co-adsorption forming a new Si-O-Ni species with the liberated Si-O bond (see Figure S9, the Si-O-Ni species is highlighted in yellow). These results show that the open structure of the Ti-OH site and the flexibility of the amorphous silica play an important role to favor the formation of the peroxide structure found.

The strong interaction observed between nickel and oxygen agrees with the experimental fact that the nickel particles seem to be mainly oxidized during and after the epoxidation reaction. To understand how the nickel oxidation degree affects the Ti-Ni interface behavior, one and two oxygen molecules have been absorbed on the nickel particle. Then, another oxygen molecule has been relaxed in the Ti-Ni interface leading to the peroxide structure of geometry II in Figure 13.

These structure optimizations finally show that the adsorption of up to two oxygen molecules does not exert a significant effect on the formation energy of the peroxide structure. The details of the study can be read in the Supplementary Information.

With the aim of investigating if the geometry II structure could be an intermediate of the epoxidation reaction, the hydroperoxide (TiOOH) structure represented in Figure 14 has been proposed and optimized. This structure consists of a migration of one of the oxygen atoms of the previous O-O peroxide structure (geometry II) and the formation of the titanium hydroperoxide species and a Ti-O-Ni link. This intermediate has been proposed by other authors [32,33] as the most probable intermediate for the epoxidation reaction in TS-1 and Au/TiO_2 catalyst, being the closest oxygen to Ti the one abstracted by the propylene to form the epoxide molecule.

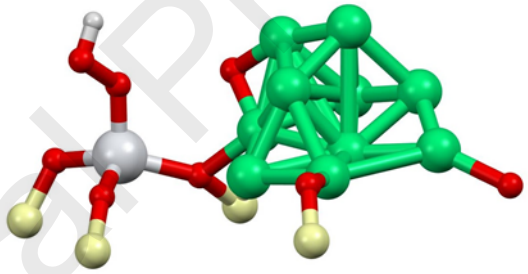

Figure 14. Optimized titanium hydroperoxide intermediate derived from geometry II structure shown in the Figure 13.

The energy calculations carried out with these two species show that the hydroperoxide structure is thermodynamically less stable than the peroxide Ti-O-O-Ni one. Therefore, the transformation from one intermediate to another results in an endothermic change of +1.18 eV, so an energy barrier higher than this energy is expected for this transformation.

In several studies [32,33] it has been proposed that the Mulliken populations of the intermediates can act as indirect indicators to evaluate the reactivity of peroxide/hydroperoxide intermediate towards epoxidation. These authors suggest that the presumed mechanism for oxygen abstraction by the olefin is the electrophilic attack of the carbon double bond. So, the oxygen atoms available should be electron deficient to be reactive.

Figure 15 shows the Mulliken charges of the two possible intermediates presented. The oxygen atom near to the Ti site that was proposed as the active oxygen in the epoxidation mechanism by gold presents populations of -0.25 and -0.28 for the TiOOH and TiOONi structures, respectively. The oxygen atoms outside the peroxide group, present Mulliken charges of -0.5 approximately, so a loss in the electron density is found in the peroxide species. This loss allows the olefin molecule to approach the oxygen without producing an electronic repulsion effect, so the electrophilic attack stated above can take place. However, the similarity in the Mulliken charges in the two structures does not give a valuable criterion to choose the most probable intermediate in the epoxidation reaction.

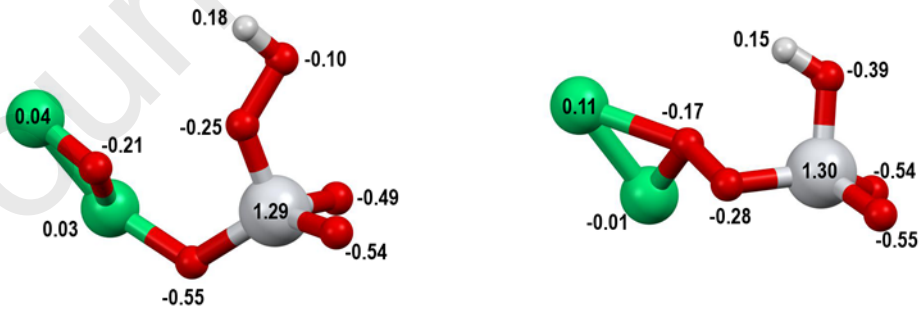

Figure 15. Mulliken populations of the two proposed intermediates.

Thus, further calculation work is being performed with the catalytic system with the aim of clarifying the mechanism of epoxidation of propylene using nickel as active metal and a Ti/SiO_2 as active site surface.

4.- CONCLUSIONS

In summary, we have studied the use of Ni-based titano-silicate catalysts for the gas-phase catalytic epoxidation of propylene. The results show excellent catalytic results under steady-state. The best catalysts (0.5% and 1% $Ni/Ti\text{-}SiO_2$) described in this work show a conversion of propylene of about 6 %, a selectivity over 85 % and a PO formation rate of 112 g $PO/(kg_{cat} \cdot h)$. These values are very interesting because (1) these are similar to the best catalysts described in the literature (Au-based $Ti\text{-}SiO_2$) being the latter the ones that have the best catalytic properties to date and (2) they use a transition metal instead of a noble metal with stable (4 h of reaction) and cyclability (3 cycles) catalytic performance. This latter advantage can reduce the cost of PO production significantly. Thus, this work can open a new route towards the use of catalysts based on non-noble metals with catalytic properties similar to Au-based catalysts in epoxidation processes. Moreover, the preliminary study done using DFT calculations with the aim of clarifying the epoxidation mechanism of propylene using nickel as active metal and a Ti/SiO_2 as support, show that the interplay between Ni and Ti species with a good interaction is very important for produce the peroxide-species intermediate which results in the production of propylene oxide, as it has been reported for the Au-based catalyst. Thus, the cornerstone for the outstanding performance of these catalysts lies in the optimization of the amount of Ni-Ti interfacial sites, which relies on the interplay between an adequate development of Ti single sites in tetrahedral coordination and a low loading of Ni on the $Ti\text{-}SiO_2$ support to avoid any detrimental Ti blocking.

ASSOCIATED CONTENT

Supporting Information. Extended computational details, the Ti 2p XPS spectra of the Ni-based catalysts, and the steady-state performance of our best reported catalyst may be found in the Supporting Information.

5.- ACKNOWLEDGMENTS

We thank the Spanish Ministry of Economy and Competitiveness (MINECO), Spanish Ministry of Science, Innovation and Universities, Generalitat Valenciana and FEDER (CTQ2015-66080-R, RTI2018-095291-B-I00, MAT2017-87579-R, and PROMETEO/2018/076) for financial support. JFC thanks MINECO for a researcher formation grant (BES-2016-078079). HR-STEM results were obtained in the installations of the DME-UCA node of the ELECMI ICTS Spanish National Infrastructure for Electron Microscopy of Materials.

6.- REFERENCES

[1] J. Huang, M. Haruta, Res. Chem. Intermed. 38 (2012) 1.

[2] S.J. Khatib, S.T. Oyama, Catal. Rev. 57 (2015) 306.

[3] B. Horváth, T. Soták, M. Hronec, Appl. Catal. A 405 (2011) 18.

[4] T. Hayashi, K. Tanaka, M. Haruta, J. Catal. 178 (1998) 566.

[5] E.E. Stangland, B. Taylor, R.P. Andres, W.N. Delgass, J. Phys. Chem. B 109 (2005) 2321.

[6] A.K. Sinha, S. Seelan, S. Tsubota, M. Haruta, Angew. Chem. Int. Ed. 43 (2004) 1546.

[7] B. Chowdhury, J.J. Bravo-Suárez, M. Daté, S. Tsubota, M. Haruta, Angew. Chem. Int. Ed. 45 (2006) 412.

[8] J. Lu, X. Zhang, J.J. Bravo-Suárez, T. Fujitani, S.T. Oyama, Catal. Today. 147 (2009) 186.

[9] M. Haruta, J. Kawahara, J. in S.T. Oyama (Ed.), Mechanisms in Homogeneous and Heterogeneous Epoxidation Catalysis, Elsevier Science, Netherlands, 2008, pp. 297–313.

[10] J. Ji, Z. Lu, Y. Lei C.H. Turner, Catalyst 4 (2018) 421.

[11] A.K. Sinha, S. Seelan, S. Tsubota, M. Haruta, Top. Catal. 29 (2004) 95.

[12] G. Mul, A. Zwijnenburg, B. van der Linden, M. Makkee, J.A. Moulijn, J. Catal. 201 (2001) 128.

[13] M.A. Barteau, R.J. Madix, J. Am. Chem. Soc. 105 (1983) 344.

[14] J.T. Roberts, R.J. Madix W.W. Crew, J. Catal. 141 (1993) 300.

[15] A. Takahashi, N. Hamakawa, I. Nakamura, T. Fujitani, Appl. Catal. A 294 (2005) 34.

[16] B. Yua, T. Ayvali, E. Raine T. Li, M.M.J. Li, J. Zheng, S. Wu, A.A. Bagabas, S.C.E. Tsang, Appl. Catal. B 243 (2019) 304.

[17] V. Duma, D. Hönicke, J. Catal. 191 (2000) 93.

[18] B. Horváth, M. Hronec, R. Glaum, R. Top. Catal. 46 (2007) 129.

[19] X. Yang, S. Kattel, K. Xiong, K. Mudiyanselage, S. Rykov, S.D. Senanayake, J.A. Rodriguez, P. Liu, D.J. Stacchiola J.G. Chen, Angew. Chem. Int. Ed. 54 (2015) 11946.

[20] J. García-Aguilar, M. Navlani-García, Á Berenguer-Murcia, K. Mori, Y. Kuwahara, H. Yamashita, D. Cazorla-Amorós, RSC Adv. 6 (2016) 91768.

[21] S. Bernal, F.J. Botana, J.J. Calvino, C. Lopez-Cartes, J.A. Pérez- Ómil, J.M. Rodríguez-Izquierdo, Ultramicroscopy. 72 (1998) 135.

[22] J. García-Aguilar, D. Cazorla-Amorós, Á. Berenguer-Murcia, Appl. Catal. A 538 (2017) 139.

[23] A. Kohlmeyer, A.; Mundy, C. J.; Mohamed, F.; Schiffmann, F.; Tabacchi, G.; Forbert, H.; Kuo, W.; Hutter, J.; Krack, M.; Iannuzzi, M.; et al. CP2K. *CP2K Developers Group* **2004**.

[24] S. Grimme, J. Comput. Chem. 27(15) (2006), 1787.

[25] J.P. Perdew, K. Burke, M. Ernzerhof, Phys. Rev. Lett. (1996) 3865.

[26] X.H. Tang, X. Wen, S.W. Sun, H.Y. Jiang, Stud. Surf. Sci. Catal. 141 (2002) 167.

[27] T. Lehmann, T. Wolff, C. Hamel, P. Veit, B. Garke, A. Seidel Morgenstern, Micropor. Mesopor. Mat. 151 (2012) 113.

[28] A.P. Grosvenor, M.C. Biesinger, C. Smart, N.S. McIntyre, Surface Science 600 (2006) 1771.

[29] B.V. Senkovskiy, D.Y. Usachov, A.V. Fedorov, O.Y. Vilkov, A.V. Shelyakov, V.K. Adamchuk, J. Alloy Compnd. 537 (2012) 190.

[30] M. Macino, A.J. Barnes, S.M. Althahban, R. Qu, E.K. Gibson, D.J. Morgan, S.J. Freakley, N. Dimitratos, C.J. Kiely, X. Gao, A.M. Beale, D.Bethell, Q. He, M. Sankar, G.J. Hutchings, Nature Catal. 2 (2019) 873.

[31] B. Taylor, J. Lauterbach, W.N. Delgass, Appl. Catal. A. 291 (2005) 188.

[32] D.H. Wells, W. Nicholas Delgass, K.T. Thomson, J. Am. Chem. Soc. 16 (2004) 2956.

[33] C.R. Chang, Y.G. Wang, J. Li, Nano Res. 4 (2011) 131.

[34] A. Roldan, D. Torres, J.M. Ricart, F. Illas, J. Mol. Catal. A Chem. 306 (2009) 6.

[35] Z.-P. Liu, P. Hu, A. Alavi, J. Am. Chem. Soc. 124 (2002) 14770.

[36] J. Guzman, B.C. Gates, J. Am. Chem. Soc. 126 (2004) 2672.

[37] B. Yoon, H. Häkkinen, U. Landman, A.S. Wörz, J.-M. Antonietti, S. Abbet, K. Judai, U. Heiz, Science 307 (2005) 403.

[38] M.S. Chen, D.W. Goodman, Science 306 (2004) 252.

[39] P. Ugliengo, M. Sodupe, F. Musso, I.J. Bush, R. Orlando, R. Dovesi, Adv. Mater. 20 (2008) 4579.

[40] D.H. Wells, W.N. Delgass, K.T. Thomson, J. Catal. 225 (2004) 69.

[41] G.W. Watson, R.P.K. Wells, D.J. Willock, G.J. Hutchings, J. Phys. Chem. B 105 (2001) 4889.

[42] D.M. Driscoll, W. Tang, S.P. Burrows, D.A. Panayotov, M. Neurock, M. McEntee, J.R. Morris, J. Phys. Chem. C 121, (2017) 1683.

[43] H.-Y. Su, X.-H. Bao, W.-X. Li, J. Chem. Phys. 128, (2008) 194707.

Graphical abstract

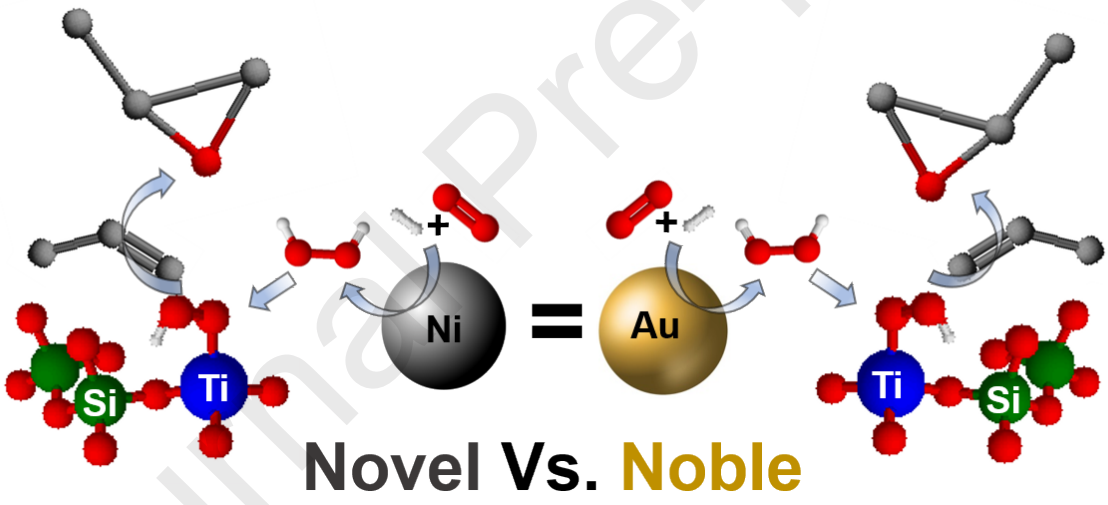

Highlights

- Ni-based catalysts have been prepared on titanosilicates by a simple route
- The prepared catalysts show outstanding propylene epoxidation performance
- DFT calculations and HRTEM have helped understand the catalysts behavior
- Formation of Ni-O-Ti interfaces is crucial to obtain efficient catalysts
- The catalysts are extremely cost-effective compared to Au-based systems